Axonal mechanisms mediating GABA-A receptor inhibition of striatal dopamine release

Paul F. Kramer[1], Emily L. Twedell[1], Jung Hoon Shin[2], Renshu Zhang[1] and Zayd M. Khaliq[1*]

[1]*Cellular Neurophysiology Unit, National Institute of Neurological Disorders and Stroke, National Institutes of Health.*

[2]*Laboratory on Neurobiology of Compulsive Behaviors, National Institute of Alcohol Abuse and Alcoholism, National Institutes of Health.*

Address for Correspondence:

Zayd M. Khaliq
Cellular Neurophysiology Unit
National Institute of Neurological Disorders and Stroke
National Institutes of Health
Bethesda, MD, 20892

Phone: 1-301-451-7221
Email: Zayd.khaliq@nih.gov

Abstract

Axons of midbrain dopaminergic neurons innervate the striatum where they contribute to movement and reinforcement learning. Past work has shown that striatal GABA tonically inhibits dopamine release, but whether GABA-A receptors directly modulate transmission or act indirectly through circuit elements is unresolved. Here, we use whole-cell and perforated-patch recordings to test for GABA-A receptors on the main dopaminergic neuron axons and branching processes within striatum. Application of GABA depolarized axons, but also decreased the amplitude of axonal spikes, limited propagation and reduced striatal dopamine release. The mechanism of inhibition involved sodium channel inactivation and shunting. Lastly, we show that the positive allosteric modulator diazepam enhanced GABA-A currents on dopaminergic neuron axons and directly inhibited release, but also likely acts by reducing excitatory drive from cholinergic interneurons. Thus, we reveal the mechanisms of GABA-A receptor modulation of dopamine release and provide new insight into the actions of benzodiazepines within the striatum.

Introduction

Axons of midbrain dopaminergic neurons are highly complex structures that transmit reward, associative-learning, and motor control signals to terminal boutons via action potentials that trigger the release of dopamine (Aransay et al., 2015; Matsuda et al., 2009; Sulzer et al., 2016). In addition to spike transmission, dopamine neuron axons within the striatum integrate local information. For example, striatal cholinergic interneurons modulate dopamine release through activation of nicotinic receptors on dopamine neuron axons (Rice and Cragg, 2004; Zhang and Sulzer, 2004) and synchronous activation of cholinergic interneurons can directly trigger dopamine release (Cachope et al., 2012; Threlfell et al., 2012). Similarly, other receptors have been shown to modulate dopamine release such as dopamine D2 (Ford, 2014), GABA-B (Pitman et al., 2014), metabotropic glutamate (Zhang and Sulzer, 2003) and muscarinic receptors (Shin et al., 2015). These data show that direct modulation of the axon presents a powerful means of controlling striatal dopaminergic signaling in a manner that is independent of somatic processing, suggesting a degree of functional segregation between these two cellular compartments (Cachope and Cheer, 2014; Hamid et al., 2016; Mohebi et al., 2019). Understanding the mechanisms that govern local control of dopamine release within the striatum will require better mechanistic knowledge of how presynaptic receptors shape axonal excitability.

GABA has long been known to modulate striatal dopamine release (Giorguieff et al., 1978; Reimann et al., 1982; Starr, 1978) but the specific contribution of GABA-A receptors (GABA-ARs) to this process is unclear. Fast-scanning cyclic voltammetry (FSCV) studies found that antagonists of GABA-ARs reduce dopamine release through an indirect mechanism involving H_2O_2 produced downstream of AMPA receptors, suggesting that GABA-ARs enhance dopamine release (Avshalumov et al., 2003; Sidlo et al., 2008). By contrast, *in vivo* microdialysis studies have found that striatal infusions of GABA-AR antagonists lead to an increase in dopamine release, suggesting that striatal GABA-ARs inhibit dopamine release (Gruen et al., 1992; Smolders et al., 1995). Consistent with this finding, an FSCV study showed that GABA-AR activation leads to inhibition of dopamine release, but argued that the effect was indirect through GABA-B receptors located on dopamine neuron axons (Brodnik et al., 2018). A more recent

study showed that GABA-AR activation inhibits dopamine release in the absence of nicotinic receptor activation which led to the proposal that GABA-A receptors may be present on the terminals of dopaminergic neurons (Lopes et al., 2019). However, definitive evidence for this proposal is lacking.

Benzodiazepines are positive allosteric modulators of GABA-ARs that are increasingly prescribed in the United States (Bachhuber et al., 2016). These drugs have demonstrated misuse liability that in rare cases leads to a substance use disorder (Blanco et al., 2018). The mechanism of benzodiazepine reward is thought mainly to involve disinhibition of somatic firing (Tan et al., 2010). Similar to many drugs of abuse, systemically-applied benzodiazepines result in acute glutamate receptor plasticity in dopamine neurons (Heikkinen et al., 2009; Kauer and Malenka, 2007) and increase the frequency of individual dopamine release events in the striatum (Schelp et al., 2018). Unlike other drugs of abuse, however, benzodiazepines have been shown to decrease the amplitude of striatal dopamine release (Gruen et al., 1992; Schelp et al., 2018). These opposing effects suggest that benzodiazepines can differentially influence activity in the soma and release from axon terminals. In the present study, we use direct axonal recordings from main axons and branching processes within the striatum, calcium imaging, FSCV, and fluorescent sensor imaging of dopamine release to disentangle these conflicting results and to mechanistically understand the influence of axonal GABA-A receptors on the excitability of, and transmitter release from, dopamine neuron axons.

Methods

Experimental Model and Subject Details

All animal handling and procedures were approved by the animal care and use committee (ACUC) for the National Institute of Neurological Disorders and Stroke (NINDS) at the National Institutes of Health. Mice of both sexes were used throughout the study. Mice that underwent viral injections were injected at postnatal day 18 or older and were used for *ex vivo* electrophysiology and imaging 3-12 weeks after injection. The following strains were used: DAT-Cre (SJL-Slc6a3(tm1.1(cre)Bkmn/J, The Jackson Laboratory Cat#006660); Ai95-RCL-GCaMP6f-D (Cg-Gt(ROSA)26Sor(tm95.1(CAG-

106 GCaMP6f)Hze)/MwarJ, The Jackson Laboratory Cat#028865); Ai9
107 (Gt(ROSA)26Sor(tm9(CAG-tdTomato)Hze), The Jackson Laboratory Cat#007909); TH-
108 GFP (Tg(TH-EGFP)1Gsat) NIH MMRRC; C57/Bl6J Wild Type, The Jackson Laboratory
109 Cat#000664; Ai32 (B6.Cg – Gt(ROSA)26Sor(tm32(CAG-COP4*H143R/EYFP)Hze), The
110 Jackson Laboratory, Cat#024109).

111 Method Details

112 *Viral Injections*

113 All stereotaxic injections were conducted on a Stoelting QSI (Cat#53311). Mice
114 were maintained under anesthesia for the duration of the injection and allowed to
115 recover from anesthesia on a warmed pad. The AAV9-CAG-FLEX-TdTomato (Penn
116 Vector Core), AAV-Syn-FLEX-jGCaMP7f (Dana et al., 2019), and AAV9-hSyn-dLight1.2
117 (Patriarchi et al., 2018) viruses (0.5-1 µl) were injected bilaterally into either the medial
118 dorsal striatum (X: ± 1.7 Y: +0.8 Z: -3.3) or the SNc (X: ± 1.9 Y: -0.5 Z: -3.9) via a
119 Hamilton syringe. At the end of the injection, the needle was raised at a rate of 0.1 to
120 0.2 mm per minute for 10 minutes before the needle was removed.

121 *Slicing and electrophysiology*

122 Brain slice experiments were performed on male and female adult mice of at
123 least 6 weeks in age. Mice were anesthetized with isoflurane, decapitated, and brains
124 rapidly extracted. Horizontal sections (electrophysiology, dLight, calcium imaging) or
125 coronal sections (voltammetry) were cut at 330-400 µm thickness on a vibratome while
126 immersed in warmed, modified, slicing ACSF containing (in mM) 198 glycerol, 2.5 KCl,
127 1.2 NaH_2PO_4, 20 HEPES, 25 $NaHCO_3$,10 glucose, 10 $MgCl_2$, 0.5 $CaCl_2$, 5 Na-
128 ascorbate, 3 Na-pyruvate, and 2 thiourea. Cut sections were promptly removed from the
129 slicing chamber and incubated for 30-60 minutes in heated (34°C) chamber with holding
130 solution containing (in mM) 92 NaCl, 30 $NaHCO_3$, 1.2 NaH_2PO_4, 2.5 KCl, 35 glucose, 20
131 HEPES, 2 $MgCl_2$, 2 $CaCl_2$, 5 Na-ascorbate, 3 Na-pyruvate, and 2 thiourea. Slices were
132 then stored at room temperature and used 30 min to 6 hours later. Following incubation,
133 slices were moved to a heated (33–35°C) recording chamber that was continuously
134 perfused with recording ACSF (in mM): 125 NaCl, 25 $NaHCO_3$, 1.25 NaH_2PO_4, 3.5 KCl,
135 10 glucose, 1 $MgCl_2$, 2 $CaCl_2$. Whole-cell recordings were made using borosilicate

136 pipettes (5-10 MΩ, axon; 2-3 MΩ, soma) filled with internal solution containing (in mM)
137 122 $KMeSO_3$, 9 NaCl, 1.8 $MgCl_2$, 4 Mg-ATP, 0.3 Na-GTP, 14 phosphocreatine, 9
138 HEPES, 0.45 EGTA, 0.09 $CaCl_2$, adjusted to a pH value of 7.35 with KOH. For high
139 chloride experiments, $KMeSO_3$ was substituted with KCl.

140 Perforated-patch recordings were made using borosilicate pipettes (5-10 MΩ)
141 filled with internal solution containing (in mM) 135 KCl, 10 NaCl, 2 $MgCl_2$, 10 HEPES,
142 0.5 EGTA, 0.1 $CaCl_2$, adjusted to a pH value of 7.43 with KOH, 278 mOsm. Pipette tips
143 were back-filled first with ~1 µL of internal lacking gramicidin followed by internal
144 containing either 4 - 8 (perforated-patch on the main axon) or 80 - 100 µg/mL
145 (perforated-patch in the striatum) gramicidin. Patch integrity was monitored by the
146 addition of Alexa-488 to the gramicidin-containing internal. Experiments were discarded
147 upon visual evidence of membrane rupture (Alexa-488 entering the axon).

148 To enable post-hoc reconstruction, pipette solutions in some experiments
149 included 0.1-0.3% w/v neurobiotin (Vector Labs), and 0.01 mM AlexaFluor 594
150 hydrazide or AlexaFluor 488 hydrazide. Current clamp recordings were manually bridge
151 balanced. Liquid junction potential for $KMeSO_3$ based internal solutions was -8 mV and
152 was corrected offline.

153 Electrical stimulation was evoked with tungsten bipolar electrodes (150 µm tip
154 separation, MicroProbes). For experiments where the site of electrical stimulation is
155 distal to the site of imaging or recording, electrodes were placed at the caudal end of
156 horizontal brain slices, or at the medial end of coronal slices. Stimulations were evoked
157 using an Isoflex (A.M.P.I.), amplitudes ranging from 0.1 to 75 V.

158 Pressure ejection was performed using a borosilicate micropipette pulled on a
159 horizontal puller (pipette size ~2-4 MΩ). The pharmacological agent being tested, either
160 GABA or muscimol, were added to a modified external solution containing (in mM): 125
161 NaCl, 25 $NaHCO_3$, 1.25 NaH_2PO_4, 3.5 KCl, 10 HEPES, 0.01 either Alexa 488 (for
162 experiments in DAT-Cre x Ai9 animals) or Alexa 594 (for experiments in TH-GFP
163 animals). This puffing solution was then spin filtered, loaded into the glass pipette, and
164 lowered to within 30-50 µm of the axon using a micro-manipulator. The puffing solution

was then applied onto the axon with a short pressure ejection (80 - 300 ms in duration) using a PV 820 Pneumatic PicoPump (WPI).

Fast-scan cyclic voltammetry (FSCV)

For all voltammetry experiments the methods are as follow. Cylindrical carbon-fiber electrodes (CFEs) were prepared with T650 fibers (6 µm diameter, ~150 µm of exposed fiber) inserted into a glass pipette and filled with KCl (3 M). Before use, the CFEs were conditioned with 8 ms long triangular voltage ramp (-0.4 to +1.2 and back to -0.4 V versus Ag/AgCl reference at 4 V/s) delivered every 15 ms. CFEs showing current above 1.8 µA or below 1.0 µA in response to the voltage ramp around 0.6 V were discarded. A triangular voltage ramp was passed through the fiber from -400 mV to 1200 mV, and returned to -400 mV. The ramp was run at a rate of 400 V/s, every 100 ms. Dopamine transients were evoked by a 2 ms 470 nm LED (ThorLabs) pulse every 60 seconds. Selective channel rhodopsin stimulation of dopamine neuron axons was achieved by injecting cre-dependent CoChR channel rhodopsin into the SNc *DAT-cre* transgenic animals. Peak dopamine currents were calculated from voltammograms created in Igor Pro (Wavemetrics).

For voltammetry experiments performed by J.H.S., the methods are as follows. Mice were anesthetized with isoflurane and sacrificed by decapitation. Brains were sliced in sagittal orientation at 240 µm thickness with a vibratome (VT-1200S Leica) in an ice-cold cutting solution containing (in mM) 225 sucrose, 13.9 NaCl, 26.2 $NaHCO_3$, 1 NaH_2PO_4, 1.25 glucose, 2.5 KCl, 0.1 $CaCl_2$, 4.9 $MgCl_2$, and 3 kynurenic acid. Slices were incubated for 20 min at 33 °C in artificial cerebrospinal fluid (ACSF) containing (in mM) 124 NaCl, 1 NaH_2PO_4, 2.5 KCl, 1.3 $MgCl_2$, 2.5 $CaCl_2$, 20 glucose, 26.2 $NaHCO_3$, 0.4 ascorbic acid, and maintained at room temperature prior recordings. Slices were placed in a submerged chamber perfused at 2 ml/min with ACSF at 32 °C using an in-line heater (Harvard Apparatus).

DA transients were evoked by brief light pulse (0.6-0.8 ms) through an optical fiber (200 µm/0.22 NA) connected to a 470 nm LED (2 mW; ThorLabs) delivered every 2 min. Data were collected with a modified electrochemical headstage (CB-7B/EC retrofit with 5 MΩ resistor) using a Multiclamp 700B amplifier (Molecular Devices) after being low-pass filtered at 10 kHz and digitized at 100 kHz using custom-written software

196 in Igor Pro running mafPC (courtesy of M.A. Xu-Friedman) software. Custom-written
197 analysis software in Igor Pro was used for analysis. Decay time constants were
198 obtained with a single exponential fit of the derivative of the falling phase of DA transient
199 curve.

200 *Fluorescent imaging*

201 Calcium mas measured in dopamine neuron axons of the medial dorsal striatum
202 using the GCaMP6f mouse bred with the DAT-Cre mouse, or with viral injection of CRE-
203 dependent jGCaMP7f into the SNc of DAT-cre mice. These data were combined in the
204 results. All calcium imaging experiments were performed in the presence of atropine,
205 sulpiride, hexamethonium chloride, and CGP55845. A white light LED (Thorlabs;
206 SOLIS-3C) was used in combination with a GFP filter set. A photodiode (New Focus)
207 was mounted on the top port of the Olympus BX-51WI microscope.

208 *Immunohistochemistry, clearing, confocal imaging, and neural reconstructions*

209 After electrophysiology or imaging, slices were fixed overnight in 4%
210 paraformaldehyde (PFA) in phosphate buffer (PB, 0.1M, pH 7.6). Slices were
211 subsequently stored in PB until immunostaining and cleared using a modified CUBIC
212 protocol, chosen because it does not quench endogenous fluorescence (Susaki et al.,
213 2015). For the immunostaining/CUBIC clearing, all steps were performed at room
214 temperature on shaker plate. Slices were placed in CUBIC reagent 1 for 1-2 days,
215 washed in PB 3 x 1 hour each, placed in blocking solution (0.5% fish gelatin (Sigma) in
216 PB) for 3 hours. Slices were directly placed in streptavidin-Cy5 conjugate at a
217 concentration of 1:1000 in PB for 2-3 days. Slices were washed 3 times for 2 hours
218 each and were then placed in CUBIC reagent 2 overnight. Slices were mounted on
219 slides in reagent 2 in frame-seal incubation chambers (Bio-Rad SLF0601) and
220 coverslipped (#2 glass). Slices were imaged through 20×, 0.8 nA and 5×, 0.3 nA
221 objectives on an LSM 800 confocal microscope (Zeiss), and taken as tiled z-stacks
222 using Zen Blue software in the NINDS light imaging facility.

223 Main axons were reconstructed and measured using Simple Neurite Tracer in
224 FIJI (Longair et al., 2011). Of axons with a positively identified soma, the majority were

225 found in the substantia nigra *pars compacta*, with some found in the ventral tegmental
226 area. Striatal axons were reconstructed using Neurolucida (MBF bioscience).

227 *Drugs*

228 All salts and all drugs not otherwise stated were from Sigma-Aldrich. Fluo5F and
229 Alexa594 (Life Technologies), gabazine, d-AP5, hexamethonium chloride, oxotremorine
230 M, GABA, and muscimol, were dissolved in deionized water. Sulpiride, quinpirole,
231 picrotoxin, CGP55845 (Tocris), NBQX, and diazepam were dissolved in DMSO.
232 Atropine was dissolved in DMSO and then diluted 1:10 in deionized water.

233 Quantification and Statistical Analysis

234 Analysis was conducted in Igor Pro and Prism 8 (GraphPad). Data in text is
235 reported as mean ($\bar{x}$) ± SEM for parametric or median ($\tilde{x}$) for non-parametric data. Error
236 bars on graphs are indicated as ± SEM. Box plots show medians, 25 and 75% (boxes)
237 percentiles, and 10 and 90% (whiskers) percentiles. For parametric data, t-tests were
238 used for two-group comparison, and ANOVA tests were used for more than two group
239 comparisons, followed by a Bonferonni or Šidák post-hoc test for analysis of multiple
240 comparisons. For non-parametric data sets, Mann-Whitney U tests were used to
241 compare two groups while the Kruskal-Wallis test was used to compare more than two
242 groups. For linear regression analysis, the Straight Line analysis function was used in
243 Prism, and an extra sum-of-squares F test was performed to determine significant
244 differences in slope between data sets on the same plot, and to determine whether a
245 line or exponential decay model fits the data better. For exponential fits, the One Phase
246 Decay analysis function in Prism was used to fit a standard curve.

247

248 **Results**

249 *Characteristics of firing in DA neuron axons – main axon and striatal terminal axons*

250 Dopamine neurons of substantia nigra *pars compacta* form thin, unmyelinated
251 axons that project to the dorsal striatum through the medial fiber bundle (MFB). To
252 examine action potential firing in the main unbranching axon from adult mice, we used a
253 horizontal brain slice which preserved the connection between the cell bodies of SNc

254 dopaminergic neurons and their MFB projecting axons. Dopaminergic neuron axons
255 within the MFB were identified using the fluorescent marker proteins GFP or td-Tomato
256 from TH-GFP mice or DAT-CRE x Ai9, respectively. Using these optimized brain slices
257 in combination with marker mice enabled us to record propagating action potentials
258 from the main axon at distances of greater than 2 millimeters from the soma (Figure
259 1A).

260 To examine the characteristics of axonal action potentials, we made whole-cell
261 recordings from the cut ends of axons (blebs) located on the surface of the slice (Hu
262 and Shu, 2012; Hu et al., 2009; Shu et al., 2007). We found that many axons exhibited
263 spontaneous firing activity with median spontaneous rates that were nearly identical to
264 somatic pacemaker rates (Figure 1B; axon: $\tilde{x}$=3.3 Hz, n=41; soma: $\tilde{x}$=2.75 Hz, n=10;
265 Mann-Whitney U test, *U*=161, p=0.298), consistent with the slow, rhythmic firing
266 associated with dopaminergic neurons (Grace and Bunney, 1984). Axonal action
267 potentials had narrower half-widths (Figures 1C and D ; axon: $\tilde{x}$=0.89 ms n=27, soma:
268 $\tilde{x}$=1.24 ms n=10; Mann-Whitney *U*=59, p=0.008 two-tailed) and a more hyperpolarized
269 threshold relative to somatic spikes (Figure 1E; axon: $\tilde{x}$=-56 mV, n=26; soma: $\tilde{x}$=-41.7
270 mV n=10; *U*=9, p<0.0001).

271 In the axon, the voltage trajectory between action potentials was shallow in slope
272 (avg. dV/dt at middle 50% of the interspike interval, axon: $\tilde{x}$=9.24 mV/s, n=27), reaching
273 a minimum at the spike trough with little depolarization before reaching threshold. By
274 contrast, the somatic interspike voltage exhibited a significantly greater slope on
275 average (Figure 1F; avg. dV/dt, soma: $\tilde{x}$=49.9 mV/s n=10; *U*=22, p<0.0001), similar to
276 previously reported values (Khaliq and Bean, 2008). A plot of the slope of the interspike
277 voltage against the axonal recording distance followed a roughly exponential
278 relationship with the interspike slope, such that it becomes more shallow with increasing
279 recording distance (Figure 1G; single exponential fit, length constant, λ=211 μm, n=27;
280 R^2=0.70; data were fit with a single exponential significantly better than with a line:
281 F(1,24)=22.1, p<0.0001). Axonal recordings at distances greater than two length
282 constants from the soma (> 422 μm) exhibited little sub-threshold depolarization
283 between action potentials ($\tilde{x}$=7.3 mV/s, n=13). In sum, action potentials recorded in the

Figure 1

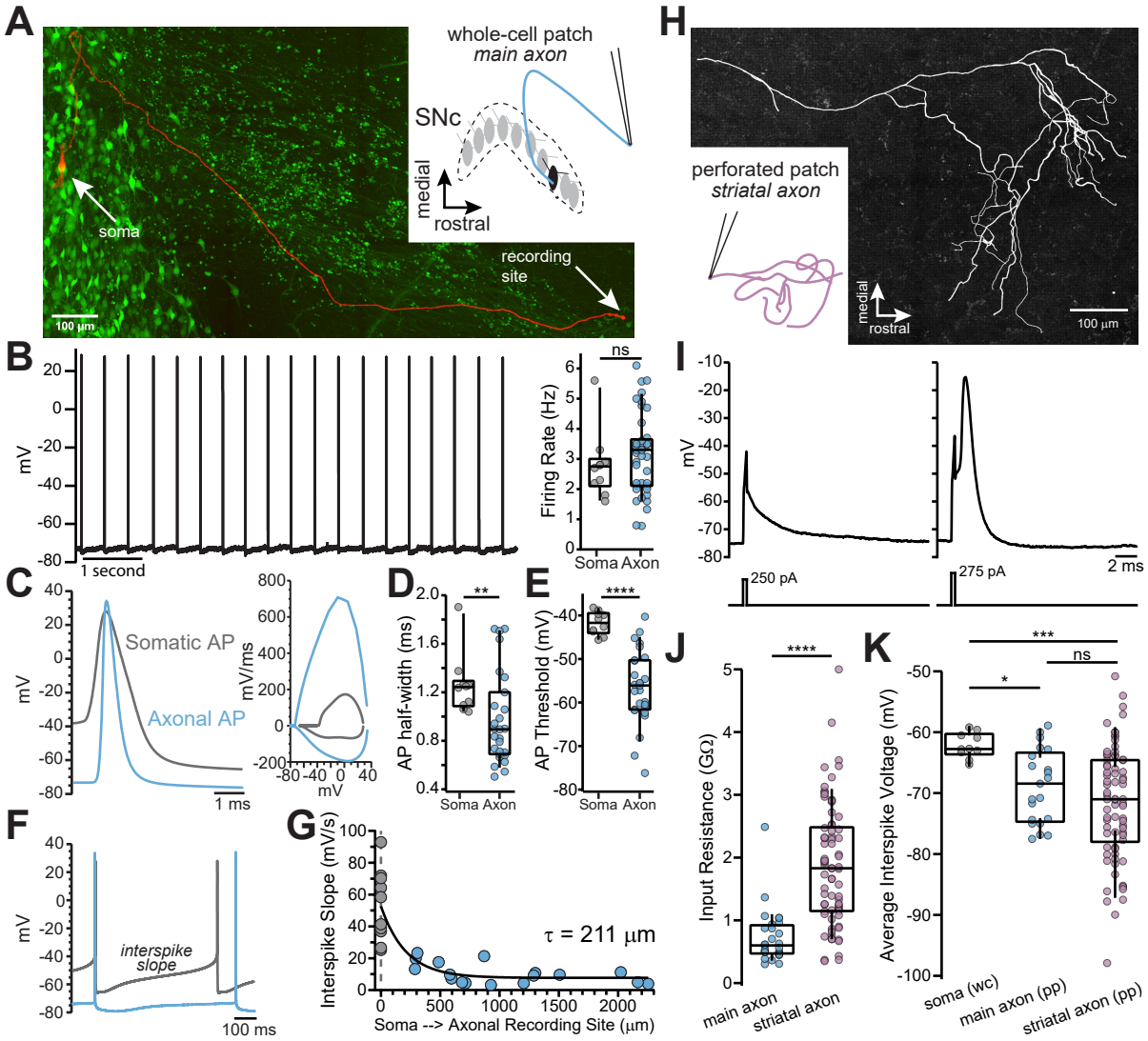

Figure 1: Whole-cell and perforated-patch recordings from dopamine neuron axons
A. Main axon recorded in whole-cell mode with a connected soma (filled with neurobiotin, imaged with streptavidin-Cy5, slice cleared with CUBIC, *red*); GFP driven by the TH promoter (*green*). **B.** Trace of spontaneous action potentials recorded from a dopaminergic axon (*left*). Firing rate from somatic (n=10) and axonal recordings (n=41; p=0.298) (*right*). **C.** Overlay of an axonal and somatic spike (*left*). Phase plot for a somatic and axonal action potential (*right*). **D.** Half-peak width from somatic (n=10) and axonal (n=27) APs (**p=0.008) **E.** AP threshold between soma (n=10) and axon (n=26)(****p<0.0001) **F.** Example traces of interspike voltage from obtained from axonal (*blue*) and somatic (*gray*) recordings. **G.** Slope of interspike voltage plotted against recording distance between axonal recording site (*blue*) and soma (*gray*). **H.** Post-hoc reconstruction of a patched striatal axon **I.** Trace of subthreshold depolarization (*left*) and axonal AP (*right*) evoked by 250 pA and 275 pA current injection. **J.** Input resistance values for main axon (n=28) and striatal axons (n=74) APs (****p<0.0001) **K.** Comparison of the mean interspike voltage between soma (n=10) main axon (n=21) and striatal axon, which was measured as the average resting membrane potential (n=74) (*p=0.032; ***p=0.0007; ns p=0.87).

Figure Supplement 1: Animated rotating movie of a striatal filled axon
Reconstructed in Neurolucida

284 main axons of dopaminergic neurons are narrow, with voltage thresholds that are
285 negative relative to somatic spikes.
286 Within the dorsal striatum, the axons of dopaminergic neurons branch
287 extensively and decrease in diameter (Matsuda et al., 2009) which raises the question
288 of how the properties of striatal terminal axons compare to those of the main axon.
289 Using perforated-patch recordings to record from axon blebs, we found that terminal
290 axons have a higher input resistance (Figure 1J; $\tilde{x}$=1.83 GΩ, n=74) than the main axon
291 ($\tilde{x}$=599 MΩ, n=28, *U*=254, p<0.0001 two-tailed). The interspike membrane potential in
292 the striatal dopamine neuron axon was hyperpolarized relative to the main axon, but
293 both axonal compartments were more hyperpolarized relative to the average interspike
294 voltage in the soma (Figure 1K; terminal axon: $\tilde{x}$=-71 mV, main axon: $\tilde{x}$=-68.9 mV,
295 soma=-62.2 mV; Kruskal-Wallis H test $\chi^2(2)=13.9$, p=0.001; terminal vs. main p=0.87;
296 terminal vs. soma, p=0.0007; soma vs. main, p=0.032). Together, these results show
297 that the main and terminal axons of dopamine neurons are high input resistance
298 compartments in which action potentials are evoked from relatively hyperpolarized
299 interspike voltages.
300
301 *Identification of GABA-A receptor-mediated currents on dopaminergic neuron axons*
302 Past work has shown that GABA-A receptors modulate dopamine release but
303 evidence that GABA-A receptors are located on dopaminergic neuron axons has been
304 indirect. To test for a GABA-A receptor-mediated conductance in the axon, a second
305 pipette was placed 30-60 µm from the axonal recording site on the main axon and
306 GABA (300 µM-1 mM) was locally applied by a brief (80-300 ms) pressure ejection
307 (Figure 2A, B). GABA puff resulted in depolarization of the axonal membrane potential
308 by an average of 4.86 ± 0.66 mV (n=9), which was completely blocked by the GABA-A
309 antagonist picrotoxin (Figure 2C; 100 µM; t(8)=6.1, p=0.0003). To verify the direct nature
310 of these currents, we tested the effect of increasing the concentration of intracellular
311 chloride on the GABA-mediated depolarization. We found that filling axons with an
312 internal solution containing high chloride resulted in GABA-mediated depolarizations
313 that were 2.76-fold larger in amplitude (Figure 2D; low Cl^-=4.74 ± 0.66 mV, high Cl^-=13.1

Figure 2

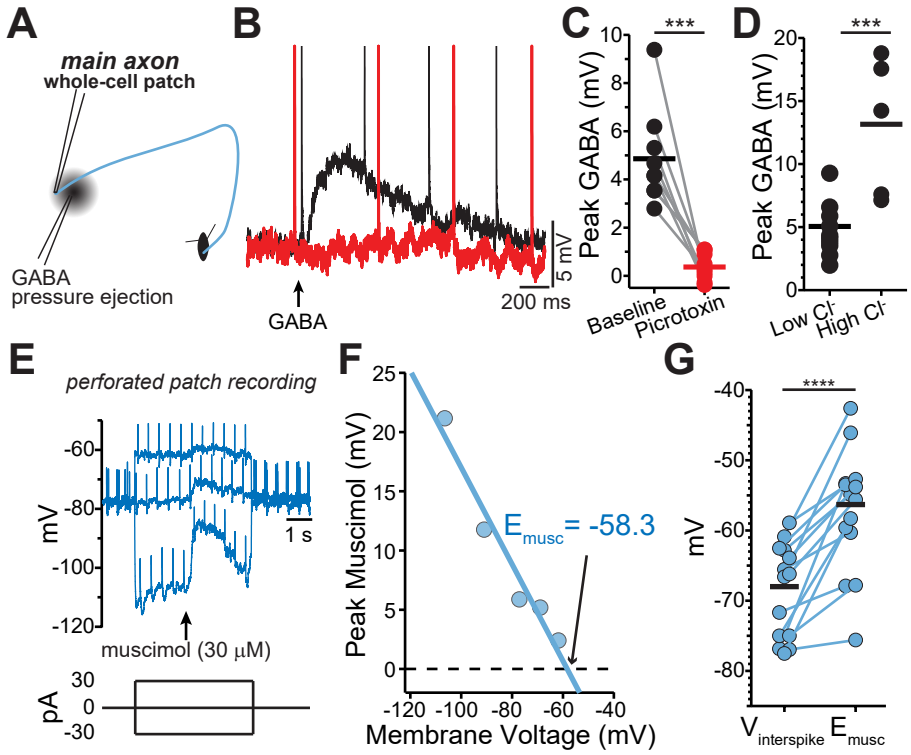

Figure 2: GABA-A receptors located on the axons of dopaminergic neuron are depolarizing

A. Schematic of experimental setup **B.** Example traces of pressure ejection of GABA onto the axon in control (*black*) and after application of picrotoxin (*red*) **C.** Peak of amplitude of GABA-evoked depolarization in control and after picrotoxin (*n*=9; ***p=0.0003) **D.** Peak amplitude of GABA-evoked depolarization recorded with low (*n*=5) or high (*n*=10) chloride internal solutions (***p=0.0008) **E.** Example traces overlaid from three different current injections. Timing of muscimol puff application indicated by *arrow* **F.** Peak of the muscimol-evoked depolarization plotted against the average interspike voltage. *Fitted line* was used to determine the reversal potential **G.** Paired values indicating mean interspike voltage ($V_{interspike}$) and muscimol reversal potential (E_{musc}) in individual axons (*n*=15; ****p<0.0001).

314 ± 2.44 mV; t(13)=4.34, p=0.0008). These results provide direct evidence for the
315 presence of functional GABA-A receptors on the axons dopaminergic neurons.
316
317 *Axonal GABA-A receptors are depolarizing*
318 The physiological function of GABA-A receptors is closely tied to its reversal
319 potential, which has been shown to vary in axons across cell types from depolarizing
320 (Pugh and Jahr, 2011; Ruiz et al., 2010; Szabadics et al., 2006) to hyperpolarizing
321 (Rinetti-Vargas et al., 2017; Xia et al., 2014). Therefore, we determined the GABA-A
322 reversal potential in the main dopaminergic neuron axons using perforated-patch
323 recordings in which the intracellular chloride concentration is preserved. While holding
324 the axon at different membrane voltages with constant current, we applied single puffs
325 of the GABA-A selective agonist muscimol and then measured the amplitude of the
326 resulting muscimol-evoked membrane depolarization (Figure 2E-G). Our analysis
327 showed that the average GABA-A reversal potential in dopamine neuron axons was -
328 56.3 ± 2.38 mV (n=15). Importantly, we found in all recorded axons that the reversal
329 potential of axonal GABA-A current was always depolarized relative to the average
330 interspike voltage of the axon (Figure 2E-G; $V_{interspike=}$-68 ± 1.75 mV, p<0.0001).
331
332 *Stronger effect of GABA-A inhibition on APs that undergo propagation*
333 Based on our finding that GABA-A receptors are depolarizing, we next
334 hypothesized that activation of axonal GABA-receptors should enhance dopamine
335 release. Therefore, we tested the effect of axonal GABA-A receptors on dopamine
336 release using fast-scan cyclic voltammetry to measure extracellular dopamine in dorsal
337 striatum slices. Dopamine release was evoked selectively from dopaminergic fibers
338 using expression of the channelrhodopsin variant, CoChR. Surprisingly, we found that
339 muscimol suppressed dopamine release from axons within the dorsal striatum. Brief
340 puff application of muscimol (10 μM, 1-3 s) resulted in an inhibition of dopamine release
341 by an average of 19.1 ± 4.2% (Figure 3A-C; control, $\bar{x}$=94.7%; muscimol, $\bar{x}$=75.7%; F(1,
342 6)=20.7, p=0.004; n=7 slices).
343 Our data show an inhibitory effect of axonal GABA-A conductance on dopamine
344 release that differs from the excitatory actions of GABA-A receptors observed in most

Figure 3

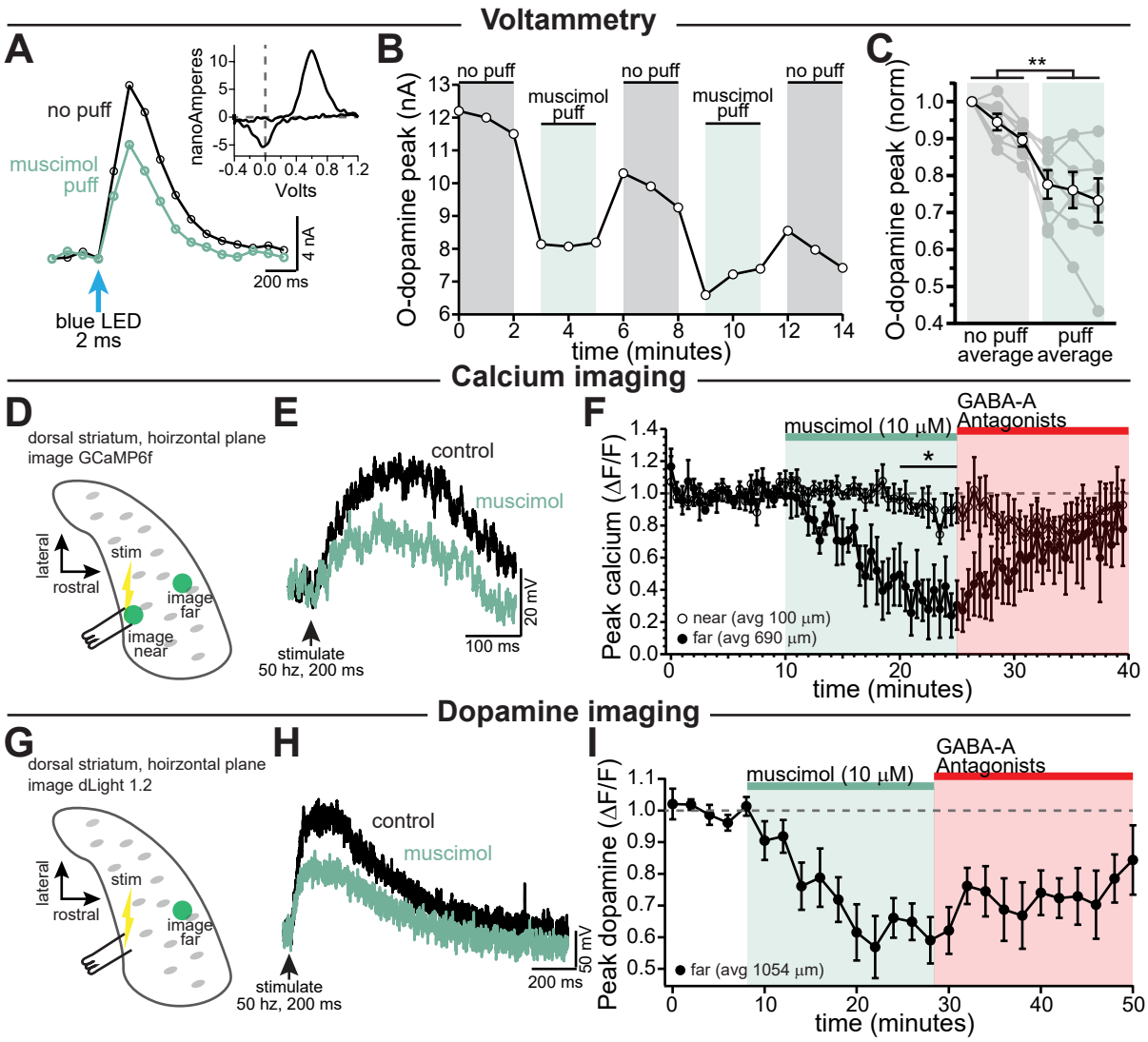

Figure 3: GABA-A receptor mediated inhibition of axonal calcium signals and striatal dopamine release

A-C. Voltammetry experiments using opsin-evoked dopamine release (DAT-Cre injected with CoChR in SNc). **A.** Example voltammetry signal of dopamine in control (*black*) and during muscimol puff (*green*). *Inset:* example current-voltage plot of FSCV signal. **B.** Time course of opsin-evoked dopamine release in an example experiment. **C.** Summary data showing the main effect of muscimol puff on dopamine release measured with voltammetry. *Closed symbols* indicate individual experiments and *open symbols* indicate averaged data (p=0.004; *n*=7) **D-F.** Stimulation-evoked calcium signals in dopamine neuron axons. **D.** Experimental setup diagram **E.** Stimulation-evoked GCaMP6f signals in control (*black*) and in response to muscimol bath application (*green*). **F.** Time course comparing the effect of bath applied muscimol for GCaMP6f signals imaged near to (average 100 μm, *n*=5) and far from (average 690 μm, *n*=5; *p=0.046) the stimulation site. **G-I.** Imaging dopamine release in the dorsal medial striatum using dLight 1.2. **G.** Experimental setup diagram. **H.** Example traces of bulk dopamine release following electrical stimulation in control (black) and during muscimol bath application (green). **I.** Group data showing the time course of muscimol application on dopamine release peak amplitude measured far from the site of stimulation (average 1054 μm, *n*=9; p=0.0008). All experiments in **D-I** were done in the presence of hexamethonium chloride (200 μM).

central axons. As one possible explanation, dopamine neuron axons in the dorsal striatum are distinguished by their highly branched structure (Matsuda et al., 2009) which under some circumstances may present a challenge for the reliability of spike propagation. We therefore set out to determine the influence of GABA-A receptors on signals that have propagated through the extreme architecture of the dopaminergic neuron terminals. To test this idea, a stimulating electrode was placed at the caudal end of the striatum, and a burst of stimulations were elicited with a bipolar electrode (Figure 3D-F). Rises in axonal calcium were recorded either near the site of stimulation ($\bar{x}$ ~ 100 μm) or far from the site of stimulation ($\bar{x}$ ~ 690 μm). Calcium increases recorded far from the site of stimulation were significantly more inhibited by activating GABA-A receptors than those recorded nearby (Figure 3F, near $\bar{x}$=94.8%, far $\bar{x}$=36.7% of baseline; Šidák's post-hoc test t(6)=3.3; p=0.046; n=5 slices for each condition).

Finally, to test the effect of GABA-A receptor activation on dopamine release for propagating action potentials, a stimulating electrode was placed at the caudal end of the striatum, and a burst of stimulations were elicited with a bipolar electrode (Figure 3G-I). Using dLight 1.2, dopamine release was measured distal to the site of stimulation ($\bar{x}$ ~ 1054 μm). Bath perfusion of muscimol (10 μM) depressed dopamine release by an average of 38.2 ± 6.6% (Figure 3I; baseline $\bar{x}$=100%, muscimol $\bar{x}$=61.8%; RM 1-way ANOVA F(2, 26)=16.5; Bonferroni's post-hoc t(8)=5.8, p=0.0008). Together, these results suggest that GABA-A receptor activation inhibits dopamine release, and acts more strongly on signals that propagate long distances through the axonal arbor.

Axonal GABA-A receptors inhibit through a combination of Na_V channel inactivation and shunting

To better understand how axonal GABA-A receptors inhibit dopamine release, we tested the effect of GABA-A receptor activation on axonal action potential waveforms. As shown in Figure 4A, the most prominent effect of GABA-A receptor activation was a shortening of the action potential peak. Although the effect of GABA on spike height varied between axons, we found that the peak was shortened on average by 7.74 ± 1.83 mV (avg. peak amplitude; control, $\bar{x}$=12.5 ± 4.72 mV; GABA, $\bar{x}$=4.77 ± 5.22 mV; 2-way ANOVA Bonferroni's post-hoc t(12)=5.75; n=7, p=0.0002). This effect

376 was blocked completely by picrotoxin (peak reduction in picrotoxin; control peak, $\bar{x}$=-
377 1.86 ± 5.34 mV, GABA peak $\bar{x}$=-3.88 ± 5.02 mV; 2-way ANOVA Bonferroni's post-hoc
378 t(12)=1.49; n=7, p=0.32). We took advantage of the variability between axons in their
379 responses to GABA in order to assess the relationship between the GABA-A mediated
380 depolarization and spike height. Plotting data from 14 axon recordings, we found that
381 the reduction in spike height correlates linearly with the GABA-mediated depolarization
382 with a slope of -1.50 mV/mV (95% CI: -2.05 to -0.94; R^2=0.74, n=14; Figure 4C, fit to
383 green symbols). Therefore, larger GABA-induced subthreshold depolarizations result in
384 shorter axonal action potentials.
385 The GABA-A mediated reduction of spike amplitude likely involves two main
386 processes: inactivation of axonal sodium channels due to GABA-induced depolarization
387 (Debanne, 2015) and shunting inhibition (Xia et al., 2014; Cattaert and El Manira, 1999).
388 To dissect the contribution from these two processes, we compared the GABA puff
389 experiments in Figure 4A to separate experiments where depolarization was evoked
390 instead by direct current injection (Figure 4B). We reasoned that the effects of current
391 injection-evoked depolarization on spike height should be dominated by sodium channel
392 inactivation whereas shunting inhibition should be minimal under these conditions.
393 Plotting the spike height against current injection-evoked depolarization in Figure 4C
394 (brown symbols), we found that direct current injections were significantly less effective
395 at reducing spike peak amplitudes as compared to GABA mediated depolarization as
396 revealed by shallower slope of best-fit lines (Figure 4C; GABA-A activation: -1.50
397 mV/mV, 95% CI: -2.05 to -0.94; direct depolarization: -0.77 mV/mV, 95% CI: -0.96 to -
398 0.59; F(1,25)=4.39, n=29, p=0.047). We next analyzed the rate of the rise of the action
399 potential (dV/dt) as it reflects the maximal spike-evoked sodium current. By contrast, we
400 found little difference in the effect of GABA-evoked and direct current injection-evoked
401 depolarization on the rate of rise of axonal action potentials (dV/dt). Plots in Figure 4D
402 show that both manipulations slowed the rate of rise of action potentials and shared
403 similar dependences on subthreshold depolarization (slope of linear fits; GABA-A
404 activation: -3.78 %/mV 95% CI: -5.46 to -2.10, direct depolarization: -3.20 %/mV, 95%
405 CI: -4.57 to -1.83; F (1,17) =0.35, n=21, p=0.56).

Figure 4

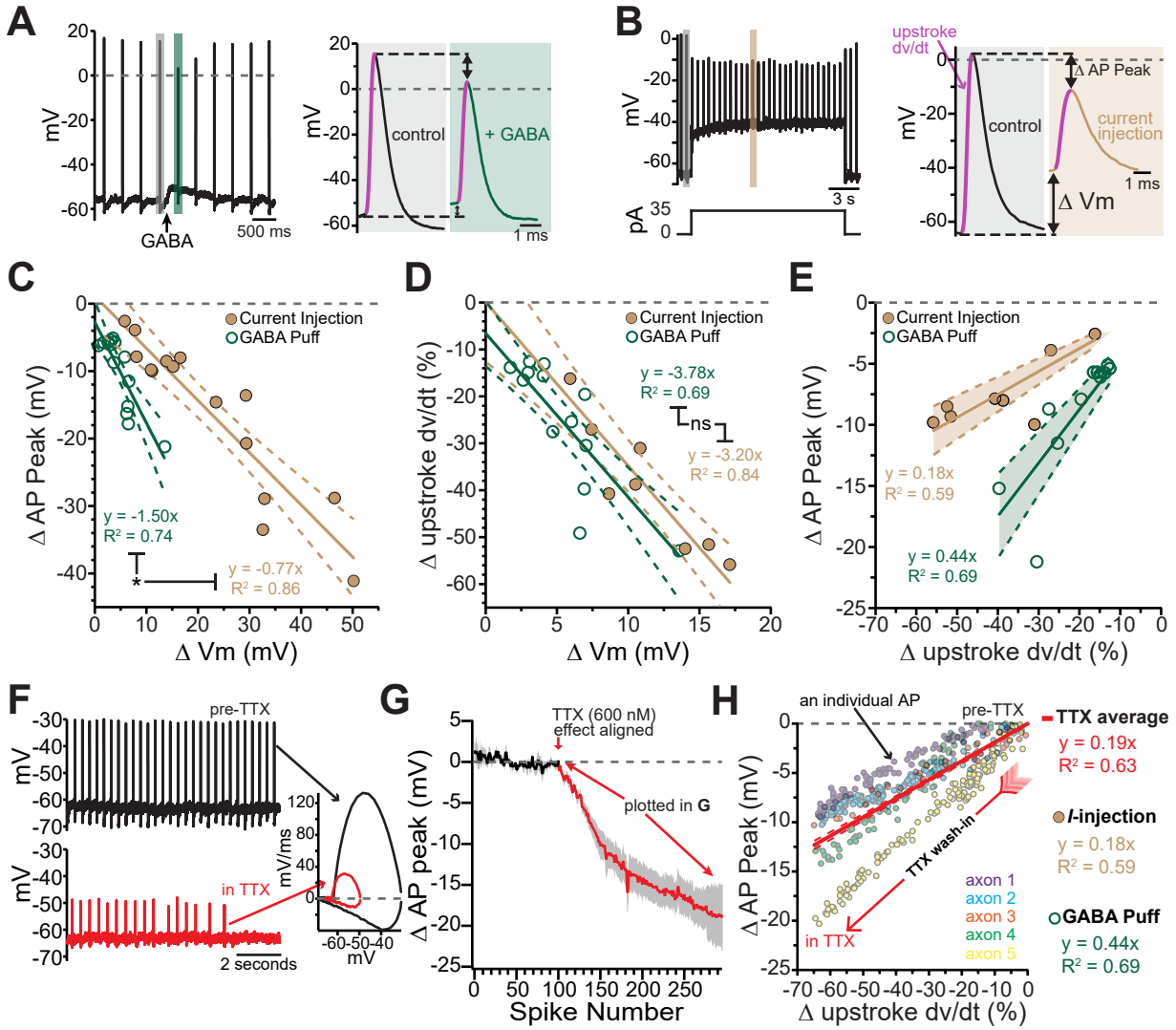

Figure 4: Axonal GABA-A receptors inhibit excitability through a combination of sodium channel inactivation and shunting

A. Example axonal recording showing the effect of a brief GABA pressure ejection. Control (grey) and GABA (green) traces magnified. *A, right:* Control action potential in black and GABA-affected action potential in green. **B.** Similar experiment to A., except demonstrating the effect current injection on spike properties as opposed to GABA application. Purple line on AP upstroke denotes area of measurement for rate of rise, arrows denoting measurement of change in AP peak and change in membrane potential **C.** Effect of the amount of baseline depolarization on the decrease in peak AP amplitude, compared between GABA (green; n=14) and current injection (tan; n=15) (*p=0.047) **D.** Effect of the amount of baseline depolarization on the normalized decrease in rate of AP upstroke, compared between GABA (green; n=11) and current injection (tan; n=10) (ns p=0.564). **E.** A plot showing the relationship between decrease in rate of AP rise and decrease in AP peak, for injection of current (brown; n=8) and a brief pressure ejection of GABA (green; n=11). **F.** Example axonal recording showing spontaneously firing action potentials before the application of TTX (*top, black)* and after TTX bath perfusion, just before the action potentials cease *(bottom, red). inset:* Example phase plots for axonal action potentials before (black) and after (red) TTX perfusion. *Right:* Averaged data showing the effect of TTX on action potential peak amplitude (graphs were aligned to the beginning of TTX effect, n=5). The decrease in peak amplitude is plotted in G. **G.** Data from five individual axons showing the effect of TTX wash-in on the change in rate of action potential rise, and the change in the peak of the action potential. Each dot in data from an individual action potential, normalized to just before the perfusion of TTX. In red is the average effect. **H.** Slope and R^2 values from **E** and **G** compared.

406 These data suggested the peak amplitude of the action potential was susceptible
407 to both depolarizations and shunting inhibition, while the rate of rise was only affected
408 by depolarizations. In order to combine these two effects and distinguish between
409 shunting inhibition and depolarization-mediated inactivation of sodium channels, the
410 change in rate of rise was graphed against the change in peak spike amplitude. From
411 this relationship the added effect of shunting inhibition is clear in the significantly
412 steeper relationship for GABA-A receptor activation (Figure 4E slope of linear fits;
413 GABA-A activation: 0.44 mV/%, 95% CI: -0.35 to 0.52, direct depolarization: 0.18
414 mV/mV, 95% CI: 0.15 to 0.22; $F(1,17) = 39.9$, $n=19$, $p<0.0001$).
415 To experimentally test the effect of sodium channel inhibition on axonal action
416 potentials, TTX was bath perfused while recording axonal action potentials (Figure 4F).
417 As the effect of TTX developed, the amplitude of the peak of the action potential was
418 progressively reduced, and the rate of rise was progressively slowed (Figure 4F-H). We
419 compared the relationship of the reduction in the peak and the slowing of the rate of rise
420 across groups and found that the average of the TTX condition was similar to the direct
421 depolarization, indicating this effect was mainly through inactivation of sodium channels.
422 However, GABA-A receptor activation had a significantly steeper relationship, revealing
423 the additional contribution of shunting inhibition (Figure 4H).
424 These data show that GABA-A receptors act mechanistically through both
425 depolarization of the axonal membrane as well as a change in the input resistance that
426 leads to shunting inhibition. These two effects combine to slow and shorten propagating
427 dopaminergic action potentials.
428
429 *Benzodiazepines enhance tonic GABA activity on dopamine neuron axons*
430 Benzodiazepines constitute a class of allosteric modulators that act on GABA-A
431 receptors to enhance GABA-mediated currents. Much is known about the somatic
432 mechanisms regulating the effects of benzodiazepines in dopamine neurons (Reynolds
433 et al., 2012; Tan et al., 2010; Tan et al., 2011); but less is known about direct axonal
434 effects of these drugs. Studies examining the effect of benzodiazepines on dopamine
435 release showed these effects are likely mediated through GABA-B receptors, and
436 indirectly involved GABA-A receptors on non-dopaminergic neurons (Brodnik et al.,

437 2018). We therefore sought to determine the contribution of GABA-A receptors on
438 dopamine neuron axons to the effects of diazepam.
439 We first tested the effect to inhibiting both GABA-A and GABA-B receptors in the
440 striatum in the absence of any exogenously applied agonist. We found that co-
441 application of GABA-A (GABAzine) and GABA-B (CGP-55845) antagonists significantly
442 enhanced dopamine release to 115% of baseline (Figure 5A, B; $t(9)=2.99$, $p=0.015$,
443 $n=10$). This finding is consistent with previous studies reporting a GABA tone in the
444 striatum (Ade et al., 2008; Gruen et al., 1992; Lopes et al., 2019).
445 We next wanted to know if diazepam acted in concert with this GABA tone to
446 inhibit dopamine release independently of GABA-B receptors. In order to isolate the
447 diazepam effect on dopaminergic axons, we recorded in a cocktail of synaptic blockers
448 targeting dopamine D2, GABA-B, muscarinic, and nicotinic receptors. While recording in
449 these antagonists, we found diazepam significantly decreased dopamine release
450 (Figure 5C; diazepam: 80.6 ± 5.9% of baseline; RM 1-way ANOVA Bonferroni's test
451 $t(5)=3.28$, $n=6$ slices; $p=0.044$). Interestingly, it has been shown that dopamine release
452 in the striatum is filtered, and can even be directly elicited, by excitatory drive from
453 cholinergic interneurons (Cachope and Cheer, 2014; Rice and Cragg, 2004; Threlfell et
454 al., 2012; Zhang and Sulzer, 2004). We were therefore curious to test how diazepam
455 affected dopamine release with cholinergic input intact. Recording dopamine release in
456 a cocktail of synaptic blockers targeting dopamine D2, GABA-B, and muscarinic, but not
457 nicotinic receptors, we found that diazepam robustly decreased dopamine release
458 (Figure 5D; diazepam: 50.7 ± 11.3% of baseline; RM 1-way ANOVA Bonferroni's post-
459 hoc $t(4)=4.37$; $p=0.024$, $n=5$ slices). The diazepam-mediated inhibition was significantly
460 greater compared to when cholinergic input was blocked (two-tailed t-test; $t(9)=2.47$,
461 $p=0.035$).
462 To understand the mechanism behind this inhibition in the dopamine neuron
463 axons we performed direct recordings from the axon. First, we sought to investigate
464 whether these axonal GABA-A receptors are directly modulated by diazepam. For this
465 experiment we puffed on muscimol in a voltage-clamp recording of the main axon, and
466 then bath perfused diazepam (10 μM). Diazepam dramatically increased the amplitude
467 of the muscimol-evoked current (Figure 5E,G). We also tested the effect of diazepam on

Figure 5

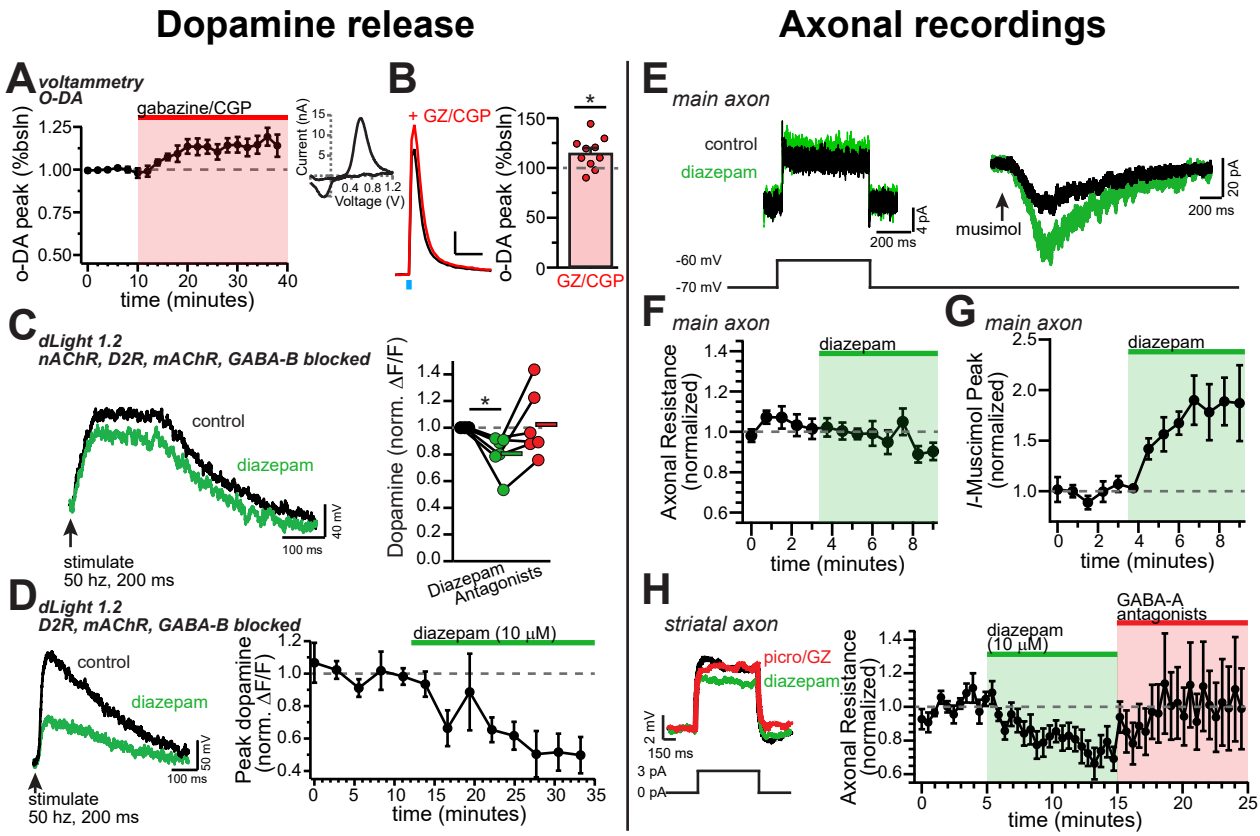

Figure 5: Diazepam inhibits striatal dopamine release through direct effects on axonal GABA-A receptors

A. GABA-A and GABA-B antagonists significantly increased the voltammetric detection of optically-evoked peak dopamine release. *Inset:* example CV plot for dopamine release. **B.** *Left:* Example dopamine transient in control (black) and in GZ/CGP (red). *Right:* Plot of the average increase in peak optically-evoked dopamine release (each dot is one slice; n=10, p = 0.015). **C.** Example traces of imaged dopamine release from control (black) and diazepam bath perfusion (green) conditions. *Right:* Group effect of diazepam on peak dopamine release (*n*=6; *p=0.044). **D.** Example traces of imaged dopamine release from control (black) and diazepam bath perfusion (green) conditions. *Right:* time course showing the effect of diazepam bath perfusion on peak dopamine release (*n*=5). **E.** Example step depolarization *(left)* and muscimol pressure ejection *(right)* recorded in the main axon in control (black) and diazepam bath application (green). Step depolarization and muscimol puff were performed within the same cell. **F.** Time course showing the effect of diazepam bath application on the normalized input resistance of the main axon in the medial forebrain bundle (*n*=5). **G.** Time course showing the effect of diazepam bath application on the normalized muscimol-evoked peak current (*n*=6). **H.** *Left:* example current injections to test axonal input resistance in control (black) diazepam (green) and GABA-A antagonists picrotoxin and GABAzine (red) conditions. *Right:* time course of diazepam bath perfusion followed by GABA-A antagonist bath perfusion on the normalized axonal input resistance.

468 the input resistance by giving a small voltage step (Figure 5E). We found that, in the
469 main axon, there was no effect of diazepam perfusion on the axonal input resistance
470 (Figure 5F). This set of experiments show that diazepam directly targets axonal GABA-
471 A receptors on dopamine neurons, but in the medial fiber bundle GABA-A agonists must
472 be exogenously applied to observe the effects of the drug.
473 Given the effect of diazepam on dopamine release reported above, we
474 hypothesized that diazepam might be acting in concert with the striatal GABA tone to
475 modulate dopamine neuron axons. When we recorded from striatal dopamine neuron
476 axons and bath perfused diazepam, we found that diazepam decreased the input
477 resistance of the axon in the striatum by an average of 22.7 ± 6.2% (Figure 5H), without
478 any additional application of a GABA agonist. These results indicate that diazepam acts
479 on the GABA tone to decrease the input resistance of dopamine neuron axons, thereby
480 potentiating shunting inhibition. These results show that diazepam directly targets
481 dopamine neuron axonal GABA-A receptors and works in concert with the striatal GABA
482 tone to modulate the input resistance of dopamine neuron axons. This mechanism
483 leads to an increased shunting inhibition and depresses stimulated dopamine release.
484

485 **Discussion**

486 Here we examine the influence of GABA-A receptors on the excitability of
487 dopaminergic neuron axons and on the release of dopamine onto targeted cells in the
488 dorsal striatum. To test this, we performed whole-cell and perforated-patch recordings
489 from the main axon located within the medial forebrain bundle as well as in the
490 branched, signaling axon located in the striatum. Using this approach, we provide direct
491 evidence that GABA-A receptors are present on the axons of midbrain dopaminergic
492 neurons. We show that these receptors modulate propagation of action potentials in the
493 axon through a combination of sodium channel inactivation and shunting inhibition.
494 Finally, we demonstrate that diazepam (Valium), a commonly prescribed broad-
495 spectrum benzodiazepine, enhances axonal GABA-A receptors which results in
496 shunting and subsequent inhibition of dopamine release. Together, these experiments
497 reveal the mechanisms of GABA-A receptor modulation of dopamine release and

498 provide new insight into the role of axonal GABA-A receptors in the actions of
499 benzodiazepines in the striatum.
500
501 **Action potential firing in midbrain dopaminergic neuron axons**
502 The shape of the axonal action potential and the pre-spike membrane potential are
503 critical determinants of neurotransmitter release (Augustine, 1990; Awatramani et al.,
504 2005; Geiger and Jonas, 2000; Rowan et al., 2016; Sabatini and Regehr, 1997). Our
505 data show that these features of axonal action potentials differ substantially from those
506 that have been classically associated with somatic firing in dopaminergic neurons
507 (Grace and Bunney, 1983; Ungless and Grace, 2012). For example, action potentials in
508 the axons of dopamine neurons are narrow with an average halfwidth of 0.89 ms, in
509 agreement with studies that have reported brief presynaptic action potentials in other
510 neuronal cell types (Alle and Geiger, 2006; Geiger and Jonas, 2000; Hallermann et al.,
511 2012; Kole et al., 2007). We also find that action potentials are initiated from spike
512 thresholds that are 14.3 mV more hyperpolarized than somatic spikes. Furthermore, the
513 average non-spike voltage recorded in both the main axon and striatal axon is 6.7 mV
514 and 8.8 mV more negative than values reported for the soma, which also fits with data
515 from cortical layer 5 pyramidal neurons (Hu and Bean, 2018).
516 The hyperpolarized axonal interspike potential has possible functional implications on
517 the control of dopamine release. First, the hyperpolarized axonal interspike voltage
518 would likely maximize the availability of low-threshold channels such as L- and T-type
519 calcium channels in axons, both of which are known to couple to dopamine release in
520 the dorsal striatum (Brimblecombe et al., 2015). Second, activation of somatodendritic
521 dopamine D2-receptors typically results in membrane hyperpolarization which then
522 raises the question of how these receptors control axonal excitability and transmitter
523 release. In the soma, D2-receptors have been shown to inhibit firing through activation
524 of G-protein activated inwardly rectifying (GIRK2) potassium channels (Beckstead et al.,
525 2004) and inhibition of the sodium leak channel NALCN (Philippart and Khaliq, 2018). In
526 axons however, D2-receptors are thought to activate Kv1 channels (Martel et al., 2011).
527 The hyperpolarized membrane potential of the axon suggests that further
528 hyperpolarization by Kv1 may be limited by the potassium reversal potential and may

529 not be the main mechanism of dopamine inhibition. Consistent with the proposal by
530 Martel and colleagues (2011), shunting and/or changes in spike shape are likely to
531 underlie the D2-dependent inhibition of dopamine release.
532 In somatic recordings of pacemaking, dopaminergic neurons exhibit a gradual
533 depolarization of the interspike voltage thought to be critical for the generation of
534 spontaneous activity (Kang and Kitai, 1993; Khaliq and Bean, 2008). By contrast, our
535 data from distal recordings show that the slope of the interspike axonal membrane
536 potential was shallow. The shallower interspike depolarization in the axon suggests that
537 pacemaking in dopaminergic neurons results largely from excitability of the soma and
538 dendrites. Furthermore, hyperpolarized axonal threshold potential suggests that our
539 recording site in the axon is distal to the site of action potential initiation, which is the
540 axon initial segment (Hausser et al., 1995; Shu et al., 2007). Therefore, these
541 observations argue against the axon as a third site of oscillation generation after the
542 soma and dendrites (Pissadaki and Bolam, 2013). It is important to note that although
543 the mixture of conductances present in axons do not favor spontaneous activity, it is still
544 possible that the conductances that drive somatic depolarization such as NALCN and
545 HCN may also be present in axons. In fact, a recent study found a positive correlation
546 between the length of the axon initial segment and the spontaneous firing rate,
547 suggesting that the axon initial segment speeds firing (Lopez-Jury et al., 2018; Meza et
548 al., 2018). However, a different study found that the geometry of the axon initial
549 segment negligibly affects the firing rate (Moubarak et al., 2019). Aside from the axon
550 initial segment geometry, future work should focus on determining the axonal
551 conductances that enable and control firing rate and spike transmission.
552
553 **Axonal GABA-A receptors on dopaminergic neuron axons are depolarizing**
554 The published literature has shown that large differences exist in the reversal
555 potential of axonal chloride-based conductances when comparing between neuronal
556 cell types. For example, a careful study of the GABA reversal potential in axon initial
557 segment of cortical layer 2/3 pyramidal neurons demonstrated that E_{GABA} shifts from
558 depolarizing to hyperpolarizing with age, eventually settling at negative values near the
559 somatic resting potential in adult mice (~ -87 mV, Rinetti-Vargas et al. (2017)). Similarly,

560 hyperpolarized GABA reversal potential values were reported from proximal axons of
561 layer 5 pyramidal neurons from rats (Xia et al., 2014). By contrast, axonal GABA-A
562 receptors on the mossy fiber bouton (Ruiz et al., 2010), cultured Purkinje neuron
563 terminals (Zorrilla de San Martin et al., 2017) as well as axonal glycine receptors on the
564 calyx of Held (Price and Trussell, 2006) have reported axonal chloride-based
565 conductances that are depolarizing relative to resting membrane potential.
566 In this study, we demonstrate that the average reversal potential of GABA-mediated
567 currents in dopamine neuron axons, when considered relative to the average axonal
568 interspike membrane potential of -68 mV, is also depolarized at -56 mV. Our recordings
569 were performed in adult mice (ages 6-17 weeks, median of 15.5 weeks) suggesting that
570 the depolarized reversal potential that we obtained represents the value in mature
571 axons. Interestingly, the reversal potential for somatodendritic GABA currents in
572 dopaminergic neurons is also depolarized at -63 mV due to relatively low expression of
573 the K-Cl cotransporter KCC2 (Gulacsi et al., 2003), which is similar to the average
574 interspike membrane potential of dopamine neurons during pacemaking. Therefore,
575 activation of somatodendritic GABA-A receptors reduces spiking primarily through
576 shunting with relatively little change in the membrane potential.
577
578 **Mechanism of axonal GABA-A receptor mediated inhibition of striatal dopamine**
579 **release**
580 Despite the depolarized GABA reversal potential in distal axons, our findings show
581 that activation of axonal GABA-A receptors results in inhibition of dopamine release.
582 Although this is consistent with work from spinal cord (Curtis and Lodge (1982); Eccles
583 et al. (1961); for a review see, Trigo et al. (2008)), these results stand in contrast to
584 previous studies that have found axonal GABA-A receptors enhance synaptic
585 transmission in cerebellar parallel fibers (Pugh and Jahr, 2011), hippocampal mossy
586 fibers (Ruiz et al., 2010), terminals of cerebellar Purkinje neurons (Zorrilla de San Martin
587 et al., 2017) and in layer 2/3 pyramidal neurons of the cortex (Szabadics et al., 2006).
588 What features distinguish dopaminergic neuron axons, and contribute to the inhibitory
589 effect of GABA-A receptors on transmitter release? The answer to this question is
590 currently unknown. However, one possibility is that dopaminergic neurons differ

591 dramatically from these other cell types in axonal architecture. For example, parallel
592 fibers and mossy fibers are unbranching. On the other hand, dopamine neuron axons
593 are among the most branching processes in the brain, forming new bifurcations an
594 average of 31 μm, and possessing an average total length of 467,000 μm (Matsuda et
595 al., 2009), from which we can estimate roughly 15,000 total branches per cell. This
596 unusually high frequency of branching may lead to stronger attenuation of propagating
597 spikes. Consistent with this, we found that activation of GABA-A receptors had only
598 subtle effects on axonal calcium signals at proximal imaging sites while axonal calcium
599 signals at distal imaging sites were dramatically reduced. Therefore, we propose that
600 GABA-A activation reduces the height of axonal action potentials which, in combination
601 with the extensive axonal branching, may have an overall effect of limiting spike
602 propagation and inhibiting dopamine release. More generally, the density of voltage-
603 gated sodium channels and other channels that support active propagation are
604 challenged by axonal GABA-A receptors, which may have a stronger effect in the thin,
605 highly branching distal axon.
606 Past studies have proposed that presynaptic GABA-A receptors exert their effects
607 through either shunting inhibition or sodium channel inactivation (Trigo et al., 2008).
608 Because of the lack of experimental access to the axonal compartment, however, direct
609 tests of this hypothesis have previously been limited to large terminal structures. In the
610 rat posterior pituitary nerve terminals, GABA was shown to produce large
611 depolarizations that led to strong inactivation of sodium channels, while shunting was
612 thought to play little role in inhibition of secretion from terminals (Zhang and Jackson,
613 1993). Here, we demonstrate in the thin, unmyelinated axons of dopaminergic neurons
614 that shunting and depolarization-mediated inactivation of sodium channels contribute
615 nearly equally to GABA-A receptor mediated alteration of action potential shape and the
616 subsequent inhibition of striatal dopamine release. Under conditions of tonic GABA-A
617 receptor activation, these two inhibitory mechanisms will be especially prominent,
618 particularly in an electrically tight compartment like the axon where tiny fluctuations of
619 GABA-A activity can cause large changes in membrane voltage and input resistance.
620 Furthermore, we found that these two mechanisms of inhibition differentially affect
621 action potential waveforms. While depolarization-mediated sodium channel inactivation

both reduces spike height and slows the rate of action potential rise, shunting inhibition only affects spike height.

Effect of benzodiazepines on axons

Benzodiazepines can have rewarding effects that, in some cases, can lead to habit formation (Blanco et al., 2018; Tan et al., 2011). The rewarding actions of benzodiazepines are thought to involve potentiation of GABA-A receptors located on inhibitory GABAergic neuron within the VTA which then results in disinhibition of VTA dopaminergic neurons (Tan et al., 2010). As is the case with other drugs of abuse that disinhibit dopamine neurons (e.g. opioids), benzodiazepines would be expected then to increase the somatic firing rate and subsequent dopamine release in the striatum. Instead, studies of awake behaving rats show that systemic diazepam administration increases the frequency of dopamine release events but decreases the amplitude of these release events (Schelp et al., 2018). The apparent disparity in these results can be reconciled by our observation that axonal GABA-A receptors on dopaminergic neuron axons are enhanced by diazepam. This enhancement of GABA-A receptors leads to a decrease in dopamine release through a combination of shunting inhibition and depolarization-mediated sodium channel inactivation. Therefore, we propose that the effects of drugs that pharmacologically target GABA-A receptors such as ethanol, barbiturates, and other sedatives should be reexamined considering their potential effects on axonal GABA-A receptors.

Previous reports examining the effect of striatal GABA tone on dopamine release have shown a main effect through GABA-B receptors (Brodnik et al., 2018; Lopes et al., 2019), with GABA-A receptors on dopamine axons lacking a clear function (Lopes et al., 2019). Our study shows that the GABA tone acts also through presynaptic GABA-A receptors located on dopamine axons. Furthermore, drugs that potentiate GABA-A receptors like diazepam will act on this tone to inhibit dopamine release. Yet, it is important to also consider that tonic GABA activity within the striatum may not only affect dopamine neuron axons. Indeed, we observed that dopamine release was more inhibited by diazepam with nicotinic receptors available rather than inhibited. This

finding hints at an additional circuit mechanism of action for diazepam, and perhaps for GABA-A receptors more generally, within the striatum. As GABA-A receptors have been found on other axons throughout the central nervous system, it is plausible to hypothesize that other neurons within the striatum also express axonal GABA-A receptors. Thus, there could be an additive effect of potentiating GABA-A receptor mediated inhibition when nicotinic receptors are available by diazepam acting through both cholinergic and dopaminergic axons.

In sum, this report shows direct evidence for GABA-A receptors on dopamine neuron axons. These receptors act mechanistically in the axon through a combination of increased shunting inhibition and sodium channel inactivation. Functionally, this results in reduced action potential propagation through the axonal arbor and decreased dopamine release, especially distal to the site of action potential initiation. Finally, benzodiazepines act directly on axonal GABA-A receptors to enhance the effects of GABA tone in the striatum, making the axons leakier and potentially weakening signal integration.

Acknowledgments

We would like to thank Dr. Veronica Alvarez (NIAAA) for input on experiments and sharing lab equipment for voltammetry experiments, and to Dr. Carolyn Smith and the NINDS Light Imaging Facility for the training and equipment to take confocal images of cleared tissue. Finally, we would like to acknowledge the Khaliq lab for their input on experiments, data presentation and the text. Funding for this research was provided by an NINDS intramural research program grant NS003134 to Z.M.K. and a Center for Compulsive Behaviors fellowship, Intramural Research Program, NIH, awarded to P.F.K.

Author Contributions

P.F.K. conducted the experiments and analyzed the data; E.L.T. conducted and analyzed immunostaining, reconstructions, and voltammetry in Figure 3. J.H.S. conducted and analyzed voltammetry experiments in Figure 5. R.Z. did the stereotaxic injections. P.F.K. and Z.M.K. designed the experiments and wrote the paper.

783

784 References

785

786 Ade, K.K., Janssen, M.J., Ortinski, P.I., and Vicini, S. (2008). Differential tonic GABA
787 conductances in striatal medium spiny neurons. J Neurosci *28*, 1185-1197.

788 Alle, H., and Geiger, J.R. (2006). Combined analog and action potential coding in hippocampal
789 mossy fibers. Science *311*, 1290-1293.

790 Aransay, A., Rodriguez-Lopez, C., Garcia-Amado, M., Clasca, F., and Prensa, L. (2015). Long-
791 range projection neurons of the mouse ventral tegmental area: a single-cell axon tracing
792 analysis. Front Neuroanat *9*, 59.

793 Augustine, G.J. (1990). Regulation of transmitter release at the squid giant synapse by
794 presynaptic delayed rectifier potassium current. J Physiol *431*, 343-364.

795 Avshalumov, M.V., Chen, B.T., Marshall, S.P., Pena, D.M., and Rice, M.E. (2003). Glutamate-
796 dependent inhibition of dopamine release in striatum is mediated by a new diffusible
797 messenger, H2O2. J Neurosci *23*, 2744-2750.

798 Awatramani, G.B., Price, G.D., and Trussell, L.O. (2005). Modulation of transmitter release by
799 presynaptic resting potential and background calcium levels. Neuron *48*, 109-121.

800 Bachhuber, M.A., Hennessy, S., Cunningham, C.O., and Starrels, J.L. (2016). Increasing
801 Benzodiazepine Prescriptions and Overdose Mortality in the United States, 1996-2013. Am J
802 Public Health *106*, 686-688.

803 Beckstead, M.J., Grandy, D.K., Wickman, K., and Williams, J.T. (2004). Vesicular dopamine
804 release elicits an inhibitory postsynaptic current in midbrain dopamine neurons. Neuron *42*, 939-
805 946.

806 Blanco, C., Han, B., Jones, C.M., Johnson, K., and Compton, W.M. (2018). Prevalence and
807 Correlates of Benzodiazepine Use, Misuse, and Use Disorders Among Adults in the United
808 States. J Clin Psychiatry *79*.

809 Brimblecombe, K.R., Gracie, C.J., Platt, N.J., and Cragg, S.J. (2015). Gating of dopamine
810 transmission by calcium and axonal N-, Q-, T- and L-type voltage-gated calcium channels
811 differs between striatal domains. J Physiol *593*, 929-946.

812 Brodnik, Z.D., Batra, A., Oleson, E.B., and España, R.A. (2018). Local GABA A Receptor-
813 Mediated Suppression of Dopamine Release within the Nucleus Accumbens. Acs Chem
814 Neurosci *10*, 1978-1985.

815 Cachope, R., and Cheer, J.F. (2014). Local control of striatal dopamine release. Front Behav
816 Neurosci *8*, 188.

817 Cachope, R., Mateo, Y., Mathur, B.N., Irving, J., Wang, H.L., Morales, M., Lovinger, D.M., and
818 Cheer, J.F. (2012). Selective activation of cholinergic interneurons enhances accumbal phasic
819 dopamine release: setting the tone for reward processing. Cell Rep *2*, 33-41.

820 Curtis, D.R., and Lodge, D. (1982). The depolarization of feline ventral horn group Ia spinal
821 afferent terminations by GABA. Exp Brain Res *46*, 215-233.

822 Dana, H., Sun, Y., Mohar, B., Hulse, B.K., Kerlin, A.M., Hasseman, J.P., Tsegaye, G., Tsang,
823 A., Wong, A., Patel, R.*, et al.* (2019). High-performance calcium sensors for imaging activity in
824 neuronal populations and microcompartments. Nat Methods *16*, 649-657.

825 Eccles, J.C., Eccles, R.M., and Magni, F. (1961). Central inhibitory action attributable to
826 presynaptic depolarization produced by muscle afferent volleys. J Physiol *159*, 147-166.

827 Ford, C.P. (2014). The role of D2-autoreceptors in regulating dopamine neuron activity and
828 transmission. Neuroscience *282*, 13-22.

829 Geiger, J.R., and Jonas, P. (2000). Dynamic control of presynaptic Ca(2+) inflow by fast-
830 inactivating K(+) channels in hippocampal mossy fiber boutons. Neuron *28*, 927-939.

831 Giorguieff, M.F., Kemel, M.L., Glowinski, J., and Besson, M.J. (1978). Stimulation of dopamine
832 release by GABA in rat striatal slices. Brain Res *139*, 115-130.

833 Grace, A.A., and Bunney, B.S. (1983). Intracellular and extracellular electrophysiology of nigral
834 dopaminergic neurons--1. Identification and characterization. Neuroscience *10*, 301-315.

835 Grace, A.A., and Bunney, B.S. (1984). The control of firing pattern in nigral dopamine neurons:
836 single spike firing. J Neurosci *4*, 2866-2876.

837 Gruen, R.J., Friedhoff, A.J., Coale, A., and Moghaddam, B. (1992). Tonic inhibition of striatal
838 dopamine transmission: effects of benzodiazepine and GABAA receptor antagonists on
839 extracellular dopamine levels. Brain Res *599*, 51-56.

840 Gulacsi, A., Lee, C.R., Sik, A., Viitanen, T., Kaila, K., Tepper, J.M., and Freund, T.F. (2003).
841 Cell type-specific differences in chloride-regulatory mechanisms and GABA(A) receptor-
842 mediated inhibition in rat substantia nigra. J Neurosci *23*, 8237-8246.

843 Hallermann, S., de Kock, C.P., Stuart, G.J., and Kole, M.H. (2012). State and location
844 dependence of action potential metabolic cost in cortical pyramidal neurons. Nat Neurosci *15*,
845 1007-1014.

846 Hamid, A.A., Pettibone, J.R., Mabrouk, O.S., Hetrick, V.L., Schmidt, R., Vander Weele, C.M.,
847 Kennedy, R.T., Aragona, B.J., and Berke, J.D. (2016). Mesolimbic dopamine signals the value
848 of work. Nat Neurosci *19*, 117-126.

849 Hausser, M., Stuart, G., Racca, C., and Sakmann, B. (1995). Axonal initiation and active
850 dendritic propagation of action potentials in substantia nigra neurons. Neuron *15*, 637-647.

851 Heikkinen, A.E., Moykkynen, T.P., and Korpi, E.R. (2009). Long-lasting modulation of
852 glutamatergic transmission in VTA dopamine neurons after a single dose of benzodiazepine
853 agonists. Neuropsychopharmacology *34*, 290-298.

854 Hu, W., and Bean, B.P. (2018). Differential Control of Axonal and Somatic Resting Potential by
855 Voltage-Dependent Conductances in Cortical Layer 5 Pyramidal Neurons. Neuron *99*, 1355.

856 Hu, W., and Shu, Y. (2012). Axonal bleb recording. Neurosci Bull *28*, 342-350.

857 Hu, W., Tian, C., Li, T., Yang, M., Hou, H., and Shu, Y. (2009). Distinct contributions of Na(v)1.6
858 and Na(v)1.2 in action potential initiation and backpropagation. Nat Neurosci *12*, 996-1002.

859 Kang, Y., and Kitai, S.T. (1993). A whole cell patch-clamp study on the pacemaker potential in
860 dopaminergic neurons of rat substantia nigra compacta. Neurosci Res *18*, 209-221.

861 Kauer, J.A., and Malenka, R.C. (2007). Synaptic plasticity and addiction. Nat Rev Neurosci *8*,
862 844-858.

863 Khaliq, Z.M., and Bean, B.P. (2008). Dynamic, nonlinear feedback regulation of slow
864 pacemaking by A-type potassium current in ventral tegmental area neurons. J Neurosci *28*,
865 10905-10917.

866 Kole, M.H., Letzkus, J.J., and Stuart, G.J. (2007). Axon initial segment Kv1 channels control
867 axonal action potential waveform and synaptic efficacy. Neuron *55*, 633-647.

868 Longair, M.H., Baker, D.A., and Armstrong, J.D. (2011). Simple Neurite Tracer: open source
869 software for reconstruction, visualization and analysis of neuronal processes. Bioinformatics *27*,
870 2453-2454.

871 Lopes, E.F., Roberts, B.M., Siddorn, R.E., Clements, M.A., and Cragg, S.J. (2019). Inhibition of
872 Nigrostriatal Dopamine Release by Striatal GABAA and GABAB Receptors. J Neurosci *39*,
873 1058-1065.

874 Lopez-Jury, L., Meza, R.C., Brown, M.T.C., Henny, P., and Canavier, C.C. (2018).
875 Morphological and Biophysical Determinants of the Intracellular and Extracellular Waveforms in
876 Nigral Dopaminergic Neurons: A Computational Study. J Neurosci *38*, 8295-8310.

877 Martel, P., Leo, D., Fulton, S., Berard, M., and Trudeau, L.E. (2011). Role of Kv1 potassium
878 channels in regulating dopamine release and presynaptic D2 receptor function. PLoS One *6*,
879 e20402.

880 Matsuda, W., Furuta, T., Nakamura, K.C., Hioki, H., Fujiyama, F., Arai, R., and Kaneko, T.
881 (2009). Single Nigrostriatal Dopaminergic Neurons Form Widely Spread and Highly Dense
882 Axonal Arborizations in the Neostriatum. The Journal of Neuroscience *29*, 444-453.

883 Meza, R.C., Lopez-Jury, L., Canavier, C.C., and Henny, P. (2018). Role of the Axon Initial
884 Segment in the Control of Spontaneous Frequency of Nigral Dopaminergic Neurons In Vivo. J
885 Neurosci *38*, 733-744.

886 Mohebi, A., Pettibone, J.R., Hamid, A.A., Jenny-Mari, T.W., Vinson, L.T., Patriarchi, T., Tian, L.,
887 Kennedy, R.T., and Berke, J.D. (2019). Dissociable dopamine dynamics for learning and
888 motivation. Nature *570*, 65-70.

889 Moubarak, E., Engel, D., Dufour, M.A., Tapia, M., Tell, F., and Goaillard, J.M. (2019).
890 Robustness to Axon Initial Segment Variation Is Explained by Somatodendritic Excitability in Rat
891 Substantia Nigra Dopaminergic Neurons. J Neurosci *39*, 5044-5063.

892 Patriarchi, T., Cho, J.R., Merten, K., Howe, M.W., Marley, A., Xiong, W.H., Folk, R.W.,
893 Broussard, G.J., Liang, R., Jang, M.J., *et al.* (2018). Ultrafast neuronal imaging of dopamine
894 dynamics with designed genetically encoded sensors. Science *360*.

895 Philippart, F., and Khaliq, Z.M. (2018). Gi/o protein-coupled receptors in dopamine neurons
896 inhibit the sodium leak channel NALCN. Elife *7*.

897 Pissadaki, E.K., and Bolam, J.P. (2013). The energy cost of action potential propagation in
898 dopamine neurons: clues to susceptibility in Parkinson's disease. Front Comput Neurosci *7*, 13.

899 Pitman, K.A., Puil, E., and Borgland, S.L. (2014). GABA(B) modulation of dopamine release in
900 the nucleus accumbens core. Eur J Neurosci *40*, 3472-3480.

901 Price, G.D., and Trussell, L.O. (2006). Estimate of the chloride concentration in a central
902 glutamatergic terminal: a gramicidin perforated-patch study on the calyx of Held. J Neurosci *26*,
903 11432-11436.

904 Pugh, J.R., and Jahr, C.E. (2011). Axonal GABAA receptors increase cerebellar granule cell
905 excitability and synaptic activity. J Neurosci *31*, 565-574.

906 Reimann, W., Zumstein, A., and Starke, K. (1982). Gamma-aminobutyric acid can both inhibit
907 and facilitate dopamine release in the caudate nucleus of the rabbit. J Neurochem *39*, 961-969.

908 Reynolds, L.M., Engin, E., Tantillo, G., Lau, H.M., Muschamp, J.W., Carlezon, W.A., Jr., and
909 Rudolph, U. (2012). Differential roles of GABA(A) receptor subtypes in benzodiazepine-induced
910 enhancement of brain-stimulation reward. Neuropsychopharmacology *37*, 2531-2540.

911 Rice, M.E., and Cragg, S.J. (2004). Nicotine amplifies reward-related dopamine signals in
912 striatum. Nat Neurosci *7*, 583-584.

913 Rinetti-Vargas, G., Phamluong, K., Ron, D., and Bender, K.J. (2017). Periadolescent Maturation
914 of GABAergic Hyperpolarization at the Axon Initial Segment. Cell Rep *20*, 21-29.

915 Rowan, M.J., DelCanto, G., Yu, J.J., Kamasawa, N., and Christie, J.M. (2016). Synapse-Level
916 Determination of Action Potential Duration by K(+) Channel Clustering in Axons. Neuron *91*,
917 370-383.

918 Ruiz, A., Campanac, E., Scott, R.S., Rusakov, D.A., and Kullmann, D.M. (2010). Presynaptic
919 GABAA receptors enhance transmission and LTP induction at hippocampal mossy fiber
920 synapses. Nat Neurosci *13*, 431-438.

921 Sabatini, B.L., and Regehr, W.G. (1997). Control of neurotransmitter release by presynaptic
922 waveform at the granule cell to Purkinje cell synapse. J Neurosci *17*, 3425-3435.

923 Schelp, S.A., Brodnik, Z.D., Rakowski, D.R., Pultorak, K.J., Sambells, A.T., Espana, R.A., and
924 Oleson, E.B. (2018). Diazepam Concurrently Increases the Frequency and Decreases the
925 Amplitude of Transient Dopamine Release Events in the Nucleus Accumbens. J Pharmacol Exp
926 Ther *364*, 145-155.

927 Shin, J.H., Adrover, M.F., Wess, J., and Alvarez, V.A. (2015). Muscarinic regulation of
928 dopamine and glutamate transmission in the nucleus accumbens. Proc Natl Acad Sci U S A
929 *112*, 8124-8129.

930 Shu, Y., Duque, A., Yu, Y., Haider, B., and McCormick, D.A. (2007). Properties of action-
931 potential initiation in neocortical pyramidal cells: evidence from whole cell axon recordings. J
932 Neurophysiol *97*, 746-760.

933 Sidlo, Z., Reggio, P.H., and Rice, M.E. (2008). Inhibition of striatal dopamine release by CB1
934 receptor activation requires nonsynaptic communication involving GABA, H2O2, and KATP
935 channels. Neurochem Int *52*, 80-88.

936 Smolders, I., De Klippel, N., Sarre, S., Ebinger, G., and Michotte, Y. (1995). Tonic GABA-ergic
937 modulation of striatal dopamine release studied by in vivo microdialysis in the freely moving rat.
938 Eur J Pharmacol *284*, 83-91.

939 Starr, M.S. (1978). GABA potentiates potassium-stimulated 3H-dopamine release from slices of
940 rat substantia nigra and corpus striatum. Eur J Pharmacol *48*, 325-328.

941 Sulzer, D., Cragg, S.J., and Rice, M.E. (2016). Striatal dopamine neurotransmission: Regulation
942 of release and uptake. Basal Ganglia *6*, 123-148.

943 Susaki, E.A., Tainaka, K., Perrin, D., Yukinaga, H., Kuno, A., and Ueda, H.R. (2015). Advanced
944 CUBIC protocols for whole-brain and whole-body clearing and imaging. Nat Protoc *10*, 1709-
945 1727.

946 Szabadics, J., Varga, C., Molnar, G., Olah, S., Barzo, P., and Tamas, G. (2006). Excitatory
947 effect of GABAergic axo-axonic cells in cortical microcircuits. Science *311*, 233-235.

948 Tan, K.R., Brown, M., Labouebe, G., Yvon, C., Creton, C., Fritschy, J.M., Rudolph, U., and
949 Luscher, C. (2010). Neural bases for addictive properties of benzodiazepines. Nature *463*, 769-
950 774.

951 Tan, K.R., Rudolph, U., and Luscher, C. (2011). Hooked on benzodiazepines: GABAA receptor
952 subtypes and addiction. Trends Neurosci *34*, 188-197.

953 Threlfell, S., Lalic, T., Platt, N.J., Jennings, K.A., Deisseroth, K., and Cragg, S.J. (2012). Striatal
954 dopamine release is triggered by synchronized activity in cholinergic interneurons. Neuron *75*,
955 58-64.

956 Trigo, F.F., Marty, A., and Stell, B.M. (2008). Axonal GABAA receptors. Eur J Neurosci *28*, 841-
957 848.

958 Ungless, M.A., and Grace, A.A. (2012). Are you or aren't you? Challenges associated with
959 physiologically identifying dopamine neurons. Trends Neurosci *35*, 422-430.

960 Xia, Y., Zhao, Y., Yang, M., Zeng, S., and Shu, Y. (2014). Regulation of action potential
961 waveforms by axonal GABAA receptors in cortical pyramidal neurons. PLoS One *9*, e100968.

962 Zhang, H., and Sulzer, D. (2003). Glutamate spillover in the striatum depresses dopaminergic
963 transmission by activating group I metabotropic glutamate receptors. J Neurosci *23*, 10585-
964 10592.

965 Zhang, H., and Sulzer, D. (2004). Frequency-dependent modulation of dopamine release by
966 nicotine. Nat Neurosci *7*, 581-582.

967 Zhang, S.J., and Jackson, M.B. (1993). GABA-activated chloride channels in secretory nerve
968 endings. Science *259*, 531-534.

969 Zorrilla de San Martin, J., Trigo, F.F., and Kawaguchi, S.Y. (2017). Axonal GABAA receptors
970 depolarize presynaptic terminals and facilitate transmitter release in cerebellar Purkinje cells. J
971 Physiol *595*, 7477-7493.
972